Impact Analysis of Concrete Wall Thermal Boundary Conditions on Fluid Outlet Characteristics Based on Transient Fluent Simulations

Shijie Zhang

School of Energy and Environmental Engineering, Hebei University of Technology, Tianjin 300401, China

Abstract. To accurately quantify the coupled relationship between Trombe wall surface thermal boundary conditions and outlet characteristics and to enhance its passive heating efficiency, this study focuses on the air channel of a Trombe wall with a concrete wall surface. Using transient numerical simulations in Fluent, we systematically investigate the influence of wall temperature ranging from 300 K to 550 K and heat flux density ranging from 200 W/m² to 400 W/m² on the outlet temperature and velocity. A laminar-flow model is established, and two sets of operating conditions—constant heat flux density and constant wall temperature—are designed. Data are obtained through numerical simulations and then fitted to develop quantitative relationship models. The results show that the outlet temperature increases significantly and linearly with both heat flux density and wall temperature, with goodness of fit $R^2 > 0.99$. The outlet velocity exhibits a nonlinear increase with heat flux density, characterized by a rapid rise followed by a more gradual growth, while it increases steadily and linearly with wall temperature (growth rate of 1.73%–2.31%). The underlying mechanism is governed by heat-transfer efficiency under the regulation of wall thermal conditions, as well as the balance between buoyancy and resistance; together, these factors synergistically determine the outlet characteristics. The four categories of quantitative models developed all achieve goodness of fit exceeding 0.99, enabling accurate prediction of outlet parameters. The findings provide reliable numerical support and a theoretical basis for optimizing the thermotechnical performance and engineering design of Trombe walls.

Keywords: Trombe wall; wall thermal boundary conditions; CFD computation; outlet characteristics; quantitative analysis.

1. Introduction

In the field of building environment and energy application engineering, the Trombe wall, as a core component of passive solar buildings, absorbs solar energy through its wall surface to heat the air within the internal air channel, thereby inducing natural convection to provide indoor heating, and it exhibits significant energy-saving potential. The heat-transfer efficiency and airflow characteristics of a Trombe wall depend directly on the wall thermal boundary conditions (temperature and heat flux density): an excessively low wall temperature leads to insufficient convective driving force, whereas an overly high wall temperature may cause indoor overheating. Moreover, non-uniform heat-flux distribution can induce fluctuations in outlet parameters, adversely affecting heating stability and thermal comfort. Traditional Trombe wall design methods based on empirical correlations struggle to accurately quantify the coupled relationship between wall thermal boundary conditions and outlet characteristics, whereas numerical simulation techniques, by constructing realistic air-channel models and visualizing airflow and heat-transfer processes, can provide accurate data support for design optimization. Therefore, investigating—based on Fluent simulations—the influence of different wall temperatures and heat flux densities on the outlet temperature and velocity of a Trombe wall is of important engineering value and theoretical significance for improving passive heating efficiency and promoting building energy conservation.

Researchers have conducted a series of studies on the heat-transfer and flow characteristics of Trombe walls, and have further carried out systematic investigations on structural innovation, material upgrading, performance optimization, and scenario adaptation, thereby producing multi-dimensional research outcomes, as summarized below:

In terms of structural innovation and functional integration, studies have focused on enhancing energy utilization efficiency through structural modification. Khaoula Friji et al. explored the thermotechnical

performance of finned Trombe walls through experiments and CFD analyses, providing data support for structurally enhanced heat transfer. Behrooz M. Ziapour et al. designed a hybrid Trombe wall coupling photovoltaics with mirrors, enabling synergy between solar power generation and space heating. Xianzhang Dong et al. developed a novel Trombe wall with solar concentrating capability, expanding pathways for energy harvesting. Tingsen Chen et al. proposed an optimization scheme coupling response surface methodology with a multi-objective particle swarm optimization algorithm to improve the overall performance of a water-based Trombe wall.

In terms of material application and performance enhancement, the integration of advanced materials has become a key direction. M. Sheikholeslami added nanoparticles into the paraffin layer of a Trombe wall to enhance the heat storage and release efficiency during phase change. Abdullah A. Abdullah et al. experimentally compared the application effects of porous media and phase change materials in PV/Trombe walls to optimize material selection. Yazi Li et al. investigated the thermal performance of Trombe walls employing multi-row channel phase change material panels, refining the application forms of phase change materials. Huabo Wu et al. developed a thermochromic hydrogel-catalytic Trombe wall, achieving integration of heat transfer and purification functions.

In terms of climate adaptation and energy-saving optimization, targeted design and system-coupling studies have been continuously advanced. Shiqiang Zhou et al., oriented to cold climate regions, conducted a parametric analysis of heating energy-saving performance for dynamic Trombe walls integrated with phase change materials. Abdullah Duzcan et al. optimized the coupled operation of phase change material Trombe walls and renewable energy systems in net-zero energy buildings. Gang Yao et al. leveraged machine learning to enable rapid prediction for Trombe wall designs of rural residences across different climate zones in China. Yafen Sun et al. examined the effects of the position of shading/insulation curtains and ventilation modes on the performance of phase change material Trombe walls, facilitating adaptation to complex climatic conditions.

In terms of fundamental performance and functional extension, fundamental parameter investigations and new function development have proceeded in parallel. Afef Laribi et al. clarified, through experiments, the influence patterns of vents on Trombe wall thermal performance. Seong Taek Kang et al., targeting buildings with limited solar resources, designed an efficient Trombe wall façade to reduce carbon emissions. Shuang-Ying Wu et al. studied the coupled effects of aspect ratio on the thermal and purification performance of photocatalytic Trombe walls. Hao Xie et al. established a thermal inactivation model for airborne bacteria and applied it to Trombe walls, extending their environmental protection functionality.

Overall, existing studies have achieved notable progress in structure, materials, and energy conservation; however, quantitative laws, coupling mechanisms, and predictive models of Trombe wall outlet characteristics under the synergistic effects of wall temperature and heat flux density remain insufficient, making it difficult to meet the requirements of refined design. To address this gap, the present study employs transient Fluent simulations to investigate the effects of wall temperature (300 K–550 K) and heat flux density (200 W/m²–400 W/m²) on outlet parameters, to reveal the coupling mechanisms, and to construct quantitative models, thereby providing theoretical and data support for Trombe wall optimization. This study takes the air channel of a Trombe wall with a concrete wall surface as the research object and conducts the following work using transient numerical simulations in Fluent: (1) based on specified thermophysical properties and actual geometric dimensions, a physical model and a numerical model of the Trombe wall air channel are established under transient conditions, and key parameters such as meshing strategy and boundary conditions are determined; (2) multiple simulation cases are designed to investigate, respectively, the transient influence of wall temperature variation under constant heat flux density and heat flux density variation under constant wall temperature on the outlet temperature and velocity; (3) quantitative relationship models between wall thermal parameters and outlet characteristics are established through data fitting.

The technical route is as follows: clarify the research objectives; construct a transient physical model based on the given thermophysical properties; set transient Fluent simulation parameters (including gravitational acceleration of −9.8 m/s²); perform transient simulations under multiple operating conditions; extract transient data and conduct plotting and tabulated analyses; discuss the mechanisms and construct models; and summarize the conclusions.

2. Numerical Simulation Theory and Model Development

2.1 Core Theoretical Basis

The transient flow and heat-transfer processes involved in this study follow the fundamental laws of fluid mechanics and heat transfer. The core governing theories include: (1) the continuity equation, which describes mass conservation of the fluid and is expressed as [1]

$$\frac{\partial \rho}{\partial t} + \nabla \cdot (\rho v) = 0$$

where ρ is the fluid density (air is taken as $1.225\ \mathrm{kg/m^3}$, under the Boussinesq assumption), t is time, and v is the velocity vector;

(2) the momentum equation, which reflects the relationship between changes in fluid momentum and external forces, incorporating gravity (gravitational acceleration $-9.8\ \mathrm{m/s^2}$) and buoyancy effects. Its vector form is [2]

$$\rho\left(\frac{\partial v}{\partial t} + v \cdot \nabla v\right) = -\nabla p + \nabla \cdot (\mu \nabla v) + \rho g,$$

where p is pressure, μ is the dynamic viscosity of air ($\mu = 1.7894 \times 10^{-5}$) (treated as a constant), and g is the gravitational acceleration vector;

(3) the energy equation, which describes energy conservation of the fluid and is given by [3]

$$\rho c_p \left(\frac{\partial T}{\partial t} + v \cdot \nabla T\right) = \nabla \cdot (\lambda \nabla T) + S_T,$$

where c_p is the specific heat capacity at constant pressure (air is taken as $1006.43\ \mathrm{J/(kg \cdot K)}$, constant; the concrete wall is taken as $936.35\ \mathrm{J/(kg \cdot K)}$, constant), T is temperature, λ is the thermal conductivity (air is taken as $0.026\ \mathrm{W/(m \cdot K)}$; the concrete wall is taken as $2.9279\ \mathrm{W/(m \cdot K)}$, constant), and S_T is the internal heat source term.

(4) the convective heat transfer between the wall and the fluid follows Newton's law of cooling [4]:

$$q = h(T_w - T_f),$$

where h is the convective heat transfer coefficient and T_f is the fluid temperature. This equation serves as the key link connecting wall thermal boundary conditions to variations in the fluid temperature.

2.2 Physical Model Construction

A Trombe wall commonly used in passive building heating systems is taken as the prototype to construct the physical model of the air flow channel, with the specific settings as follows:

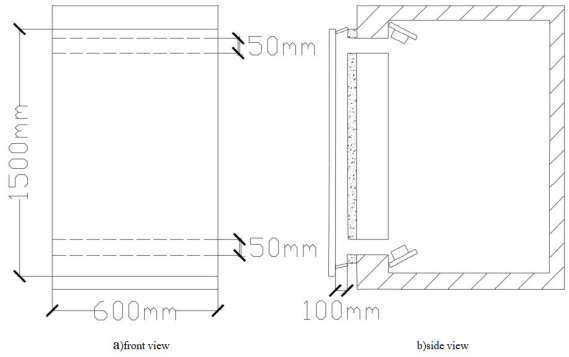

Fig. 1 Physical model of the Trombe wall air flow channel a)front view b)side view

A Trombe wall commonly used in passive building heating systems is taken as the prototype, and its air flow channel physical model is established. The channel dimensions are 100 mm in the x-direction, 1500 mm in the y-direction, and 600 mm in the z-direction, while the inlet and outlet heights are both 150 mm. The inner wall surface of the Trombe wall is made of concrete, and its thermophysical properties are treated as constants: density $2391.7\ \mathrm{kg/m^3}$, specific heat $936.35\ \mathrm{J/(kg \cdot K)}$, and thermal conductivity $2.9279\ \mathrm{W/(m \cdot K)}$. The indoor wall is made of masonry-type material and is treated as adiabatic, such that heat dissipation effects are neglected. The working fluid inside the channel is air, and the Boussinesq approximation is employed to simplify buoyancy calculations [5]. The thermophysical properties are specified as: density $1.225\ \mathrm{kg/m^3}$ (constant), specific heat $1006.43\ \mathrm{J/(kg \cdot K)}$ (constant), dynamic viscosity $1.7894 \times 10^{-5}\ \mathrm{kg/(m \cdot s)}$ (constant), and thermal conductivity $0.026\ \mathrm{W/(m \cdot K)}$.

The inlet boundary is specified as a velocity inlet, with the initial velocity $v_{in} = 0\ \mathrm{m/s}$ and the initial temperature $T_{in} = 300\ \mathrm{K}$. The outlet boundary is defined as a pressure outlet, with the gauge pressure set to 0 Pa. The concrete inner wall is treated as a no-slip boundary, and two types of thermal boundary conditions are applied, namely constant wall temperature and constant heat flux density. Transient calculations are performed, with a time step of 0.1 s; the total simulation time is determined according to the stabilization of the outlet parameters.

2.3 Numerical Model and Solution Settings

Flow-regime identification (basis for model selection). The flow regime is determined using the Reynolds number, and the core calculation procedure is as follows:

1. Definition of key parameters: The kinematic viscosity is derived from $\nu = \mu/\rho$; substituting the parameters gives $\nu \approx 1.461 \times 10^{-5}\ m^2/\mathrm{s}$. The steady local mean outlet velocity v_{out} ranges from $0.17 \sim 0.22\ \mathrm{m/s}$, and a representative value $v_{out} = 0.2\ \mathrm{m/s}$ is adopted in the calculation. The outlet cross-sectional area is $A_{out} = 0.09\ m^2$, and the total flow cross-sectional area of the channel is $A_{total} = 0.06\ m^2$.

2. Computation of the cross-sectional mean velocity: Based on the flow-rate conservation law $Q = v_{out} \cdot A_{out} = v_{avg} \cdot A_{total}$, it follows that the mean cross-sectional velocity can be written as $v_{avg} = v_{out} \cdot A_{out}/A_{total}$. Substituting the parameters yields $v_{avg} = \frac{0.2\ \mathrm{m/s} \times 0.09\ \mathrm{m^2}}{0.06\ \mathrm{m^2}} = 0.3\ \mathrm{m/s}$.

3. Reynolds number calculation and flow-regime determination: The Reynolds number is calculated as: $Re = v_{avg} \cdot d/\nu$. Substituting $v_{avg} = 0.3\ \mathrm{m/s}$, channel width $d = 0.1\ \mathrm{m}$, and $\nu \approx 1.461 \times 10^{-5}\mathrm{m^2/s}$, gives $Re = (0.3 \times 0.1)/(1.461 \times 10^{-5}) \approx 2053$. The Reynolds-number criteria for rectangular-channel flows are: laminar ($Re < 2300$), transitional ($2300 < Re < 4000$), and turbulent ($Re > 4000$). In this study, $Re \approx 2053$ falls within the laminar regime, and the channel flow exhibits no intense disturbances, which is consistent with the core characteristics of laminar flow (molecular transport dominance, strong stability, and no pronounced turbulent fluctuations). Therefore, the laminar-flow model is adopted. Governing-equation specification. The governing equations of the laminar model are formulated based on the core theory in Section 2.1 and are specified in conjunction with natural convection as follows: The continuity equation, momentum equation, and energy equation follow the core formulations given in Section 2.1. Buoyancy treatment: the Boussinesq approximation is employed, where the air density is taken as a constant $1.225\ \mathrm{kg/m^3}$, and the temperature dependence of density is reflected only in the gravity term of the momentum equation, thereby accurately representing buoyancy-driven natural convection characteristics.

4. Solver and discretization schemes

Solver: A pressure-based solver is used, and the pressure–velocity coupling is handled using the Semi-Implicit Method for Pressure-Linked Equations–Consistent

(SIMPLEC), balancing convergence speed and numerical stability.
Time discretization: A transient time-marching scheme is adopted, and a first-order implicit formulation is used to ensure computational stability and avoid oscillations.
Spatial discretization: Pressure interpolation is performed using a second-order upwind scheme, and both the momentum and energy equations are discretized using second-order upwind schemes to reduce numerical diffusion and improve computational accuracy.
5. To ensure the reliability of the simulation results, three convergence criteria are specified:
① the residuals of the continuity and momentum equations are less than 10^{-4};
② the residual of the energy equation is less than 10^{-6} (to meet the high-accuracy requirement for heat exchange);
③ the variations of outlet temperature and outlet velocity over five consecutive time steps are less than 0.1%.
When the above conditions are satisfied simultaneously, the flow field is considered to have reached a steady state; the computation is terminated and data are extracted.

2.4 Simulation Case Design

To systematically investigate the influence of wall thermal boundary conditions on the outlet characteristics of the Trombe wall, two sets of variable cases are designed: (1) varying heat-flux-density cases: the heat flux density is fixed at $q = 200\ W/m^2$, $250\ W/m^2$, $300\ W/m^2$, $350\ W/m^2$, and $400\ W/m^2$; (2) varying wall-temperature cases: the wall temperature is fixed at $T_w = 300\ K$, $350\ K$, $400\ K$, $450\ K$, $500\ K$, and $550\ K$. Transient calculations are performed with a time step of 0.1 s. The time histories of outlet temperature and velocity are recorded, and data in the steady stage are used for analysis. Each case is repeated twice to ensure the reliability of the results.

3. Influence Analysis under Varying Heat Flux Density

3.1 Variation Pattern and Analysis of the Outlet Temperature

The time histories of the outlet temperature under different heat flux densities show that, in all cases, the temperature of the air micro-parcels increases gradually with time until a steady state is reached. A higher heat flux density leads to a higher steady-state temperature of the air micro-parcels and a shorter time to reach steady state. When the heat flux density increases from $200\ W/m^2$ to $400\ W/m^2$, the steady-state outlet temperature increases linearly from 308.47 K to 315.39 K.
From the perspective of heat-transfer principles, as the heat flux density increases, the amount of heat transferred from the concrete wall to the air micro-parcels via convective heat transfer increases. According to the law of energy conservation, the heat absorbed by the air micro-parcels is converted into thermodynamic energy, and the temperature rises accordingly. Moreover, the larger the heat flux density, the greater the temperature-gradient-driven difference between the wall surface and the air micro-parcels, resulting in a stronger heat-transfer driving force and a faster rate of heat transfer, enabling the air micro-parcels to reach thermal equilibrium more rapidly; therefore, the outlet temperature stabilizes earlier. From the viewpoint of heat–mass exchange, increasing the heat flux density enhances the heat-transfer efficiency between the wall surface and the air micro-parcels, improves the heating uniformity of the air micro-parcels, and avoids local temperature fluctuations, which further ensures a stable linear increasing trend of the outlet temperature with heat flux density.

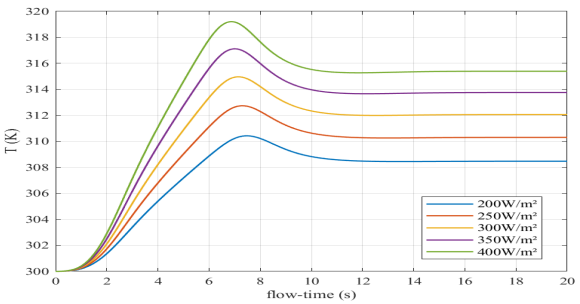

Fig. 2 Temporal evolution profiles of air microcluster outlet temperature under different heat flux densities

Note: This figure illustrates the temperature ramp-up and steady-state behavior of air microcluster outlet temperature across heat flux densities spanning 200 W/m² to 400 W/m². Elevated heat flux densities correspond to reduced steady-state attainment durations and higher asymptotic steady-state temperatures.

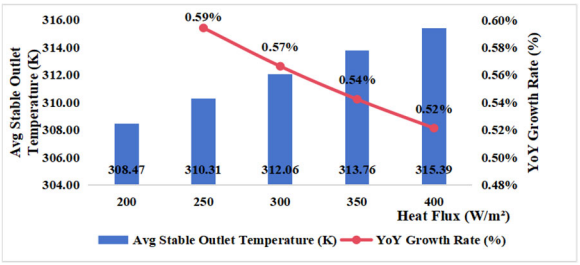

Fig. 3 Dependence of air microcluster steady-state outlet temperature and its year-on-year (YoY) growth rate on heat flux density

Note: The bar plot represents the average steady-state outlet temperature at each specified heat flux density, and the line plot denotes the corresponding year-on-year (YoY) growth rate. A linear increase in steady-state temperature is observed as the heat flux density rises from 200 W/m² to 400 W/m².

3.2 Variation Pattern and Analysis of the Outlet Velocity

The time histories of the outlet velocity indicate that, under all heat-flux-density cases, the velocity of the air micro-parcels increases with time until reaching a steady state, and a higher heat flux density corresponds to a larger steady-state velocity. A lateral comparison further shows that the outlet velocity increases with heat flux density in a pattern of "rapid increase followed by a slower rise"; the

maximum growth rate of 2.79% occurs at 250 W/m^2, after which the increment rate gradually decreases.

From the standpoint of fluid mechanics, increasing the heat flux density strengthens heat exchange between the wall surface and the air micro-parcels. After being heated, the air micro-parcels experience a decrease in density, forming a density difference relative to the higher-density air micro-parcels near the upper region of the channel that are not yet sufficiently heated. This enhances the natural-convection driving force and increases the flow velocity of the air micro-parcels. As the heat flux density continues to rise, the flow within the channel tends toward a fully developed state, leaving less room for further velocity increase. Meanwhile, the elevated temperature of the air micro-parcels slightly increases the dynamic viscosity, thereby increasing flow resistance; the combined effect of these two factors leads to a reduced growth rate. From the perspective of heat–mass exchange, a higher heat flux density promotes more uniform heat transfer, reduces temperature-distribution differences among air micro-parcels, and enhances flow stability—driving a rapid velocity increase in the early stage. In the later stage, as the flow state becomes increasingly stable, the velocity increment naturally slows down, resulting in the characteristic trend of "fast first, then slow."

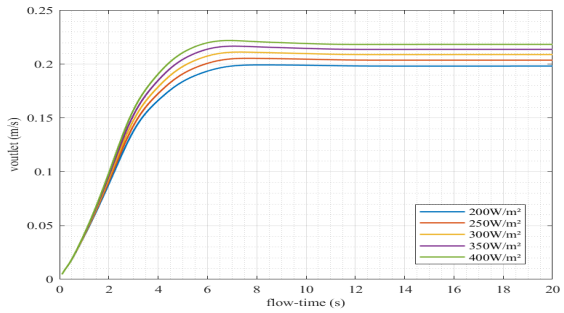

Fig. 4 Transient evolution characteristics of air microcluster outlet velocity under varied heat flux densities

Note: This figure illustrates the velocity ramp-up and steady-state behavior of air microcluster outlet velocity across heat flux densities (200 W/m² to 400 W/m²). Elevated heat flux densities correspond to accelerated velocity growth kinetics and higher steady-state terminal velocities, consistent with enhanced momentum transfer at the wall-air interface.

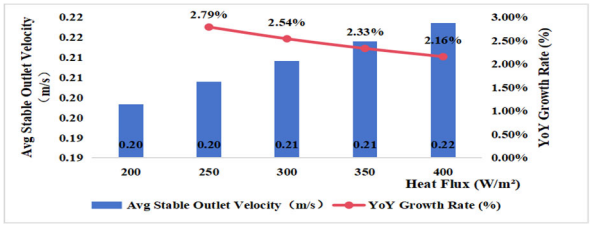

Fig. 5 Correlation between heat flux density, steady-state outlet velocity of air microclusters, and year-on-year (YoY) growth rate

Note: The bar plot denotes the mean steady-state outlet velocity at each heat flux density, and the line plot represents its YoY growth rate. As heat flux density increases, the steady-state outlet velocity rises monotonically, while the YoY growth rate exhibits a gradual downward trend—reflecting the diminishing marginal effect of heat flux on velocity enhancement.

4. Influence Analysis under Varying Wall Temperature

4.1 Variation Pattern of the Outlet Temperature

The outlet-temperature evolution curves under different wall temperatures indicate that the outlet temperature increases linearly with increasing wall temperature. For every 50 K increase in wall temperature, the outlet temperature rises by an average of 1.05 K, and a higher wall temperature corresponds to a shorter time for the outlet temperature to reach a steady state. From the perspective of heat-transfer theory, increasing the wall temperature enlarges the temperature difference between the wall surface and the air micro-parcels. According to the fundamental heat-transfer equations, the heat-transfer rate is positively correlated with the temperature difference; the larger the temperature difference, the higher the heat-transfer efficiency from the wall to the air micro-parcels, the greater the heat absorbed by the air micro-parcels, the more pronounced the increase in thermodynamic energy, and thus the temperature increases linearly. Meanwhile, a higher wall temperature can rapidly establish a stable temperature gradient within the channel, accelerating the heat-exchange process of the air micro-parcels, enabling them to reach thermal equilibrium faster and allowing the outlet temperature to stabilize earlier. From the principle of heat–mass exchange, the elevated wall temperature strengthens heat transfer between the air micro-parcels and the wall surface during convective heat exchange, leading to more uniform heating of the air micro-parcels without local overheating or underheating, which further guarantees the linear relationship between outlet temperature and wall temperature.

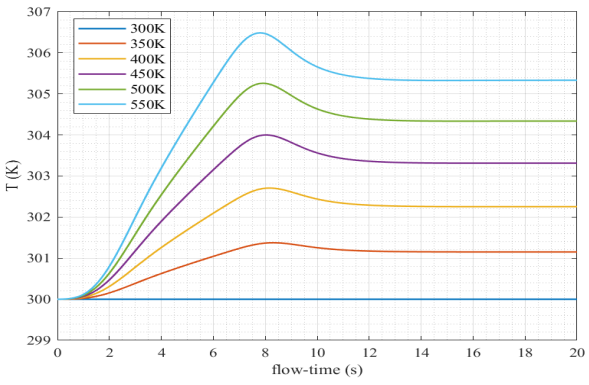

Fig. 6 Transient evolution of air microcluster outlet temperature under varied wall temperatures

Note: This figure depicts the temperature ramp-up and steady-state behavior of air microcluster outlet temperature across wall temperatures (300 K to 550 K). Elevated wall temperatures accelerate the temperature growth rate of air microclusters, with higher wall temperatures corresponding to shorter steady-state

attainment times and higher terminal steady-state temperatures (units: temperature in K, time in s).

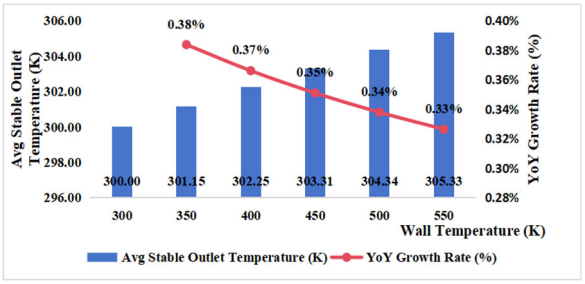

Fig. 7 Dependence of air microcluster steady-state outlet temperature and its year-on-year (YoY) growth rate on wall temperature

Note: The bar plot denotes the mean steady-state outlet temperature at each specified wall temperature, while the line plot represents its YoY growth rate. As wall temperature increases (from 300 K to 550 K), the steady-state outlet temperature rises monotonically, while the YoY growth rate exhibits a gradual downward trend—reflecting the diminishing marginal effect of wall temperature on temperature enhancement (units: temperature in K, growth rate in %).

4.2 Variation Pattern of the Outlet Velocity

The outlet-velocity curves under varying wall temperatures show that the outlet velocity increases steadily with increasing wall temperature. Under the 550 K case, the velocity reaches 0.19 m/s, with the growth rate remaining within 1.73% ~ 2.50% . From the perspective of fluid mechanics, an increased wall temperature leads to a larger thermal expansion of the air micro-parcels and a more pronounced reduction in density. The resulting density difference relative to the cold air micro-parcels in the upper region of the channel is enlarged, and the natural-convection driving force is significantly strengthened, thereby promoting a higher flow velocity of the air micro-parcels. In addition, as the density of the air micro-parcels decreases more uniformly, fluctuations in flow resistance are reduced, allowing the velocity to increase at a stable rate.

From the standpoint of heat-transfer theory, a higher wall temperature enhances heat exchange between the wall surface and the air micro-parcels, leading to a more uniform temperature distribution in the air micro-parcels, avoiding flow disturbances caused by local temperature differences, and ensuring a stable increase in velocity. Combined with the heat–mass exchange principle, increasing the wall temperature improves heat-transfer efficiency and results in a more uniform rise in the thermodynamic energy of the air micro-parcels; intensified molecular motion further facilitates the increase in flow velocity. Consequently, a consistent trend is obtained in which the outlet velocity increases steadily with wall temperature while the growth rate remains stable.

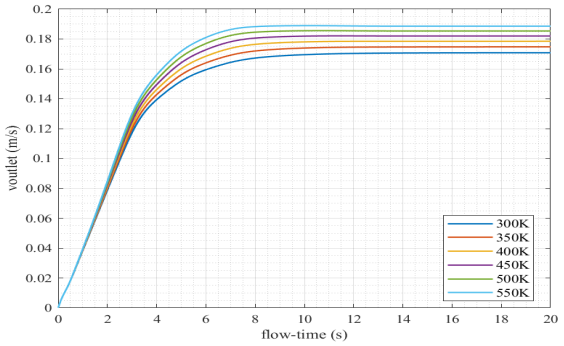

Fig. 8 Transient evolution characteristics of air microcluster outlet velocity under varied wall temperatures

Note: This figure illustrates the velocity ramp-up and steady-state process of air microcluster outlet velocity across wall temperatures (300 K to 550 K). Higher wall temperatures enhance momentum transfer at the wall-air interface, leading to faster velocity growth and elevated steady-state terminal velocities (units: velocity in m/s, time in s).

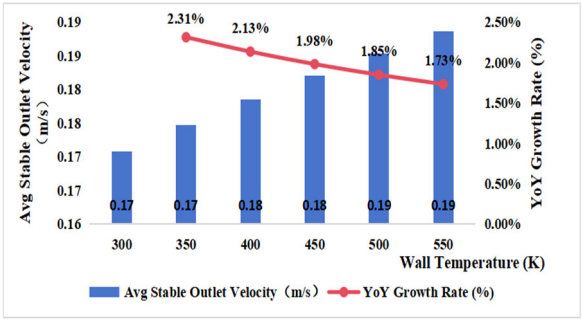

Fig. 9 Correlation between wall temperature, steady-state outlet velocity of air microclusters, and year-on-year (YoY) growth rate

Note: The bar plot represents the average steady-state outlet velocity at each wall temperature, and the line plot denotes its YoY growth rate. As wall temperature increases (from 300 K to 550 K), the steady-state outlet velocity increases gradually, while the YoY growth rate declines continuously—consistent with the weakened sensitivity of velocity to wall temperature elevation (units: velocity in m/s, wall temperature in K, growth rate in %).

5. Influence Mechanisms and Quantitative Analysis

5.1 Comprehensive Analysis of the Mechanisms Governing Outlet Characteristics

Variations in the outlet temperature and outlet velocity of the Trombe wall air channel are primarily regulated by the coupled effects of heat transfer and fluid flow under wall thermal boundary conditions. The intrinsic mechanisms can be discussed from three aspects—heat transfer, fluid motion, and the synergistic coupling between thermal and flow fields [33–35]:

(1) Mechanism affecting the outlet temperature

The variation in outlet temperature is essentially an accumulation process of thermodynamic energy in the air micro-parcels and is determined by the heat-transfer efficiency between the wall surface and the air. Under constant heat-flux-density conditions, the heat flux density directly determines the total amount of heat transferred from the wall to the air per unit time. The larger the heat flux density, the more heat the air micro-parcels absorb, the more pronounced the increase in thermodynamic energy, and the higher the outlet temperature. Moreover, because the heat flux density is linearly correlated with the heat-transfer amount, the outlet temperature increases linearly with heat flux density. Under constant wall-temperature conditions, increasing the wall temperature enlarges the heat-exchange temperature difference between the wall surface and the air micro-parcels. According to Newton's law of cooling, the heat-transfer rate increases with the temperature difference, thereby accelerating the heat-absorption rate of the air micro-parcels and leading to a linear rise in temperature. Meanwhile, the thermophysical properties of air are specified as constants, and the convective heat-transfer coefficient remains stable, which further ensures the linear relationship between outlet temperature and wall temperature. In addition, the flow state inside the channel indirectly affects the outlet temperature: a stable flow allows sufficient contact between the air micro-parcels and the wall surface, avoids locally non-uniform heat exchange, and ensures the regularity of outlet-temperature variations with changes in thermal boundary conditions.

(2) Mechanism affecting the outlet velocity

The variation in outlet velocity is governed by the balance between the natural-convection driving force and the fluid-flow resistance. Wall thermal boundary conditions modify the density distribution of air micro-parcels and generate buoyancy, which constitutes the primary driving force of the flow: either increasing the heat flux density or raising the wall temperature strengthens heat exchange between the wall and the air, increasing the temperature of the air micro-parcels and reducing their density. This produces a larger density difference relative to the comparatively low-temperature, high-density air in the upper region of the channel, significantly enhancing buoyancy and thereby increasing the air velocity. Flow resistance dynamically adjusts with velocity: as velocity increases, both frictional resistance along the flow path and local losses rise accordingly, offsetting part of the buoyancy effect. Under constant heat-flux-density conditions, when the heat flux density is relatively low, the growth rate of buoyancy exceeds that of resistance, and the outlet velocity increases rapidly. When the heat flux density exceeds $350\ \mathrm{W/m^2}$, the magnitude of density variation in the air micro-parcels decreases, causing buoyancy growth to slow, while resistance continues to increase, resulting in a gradual leveling-off of the velocity increase. Under constant wall-temperature conditions, the enhancement of buoyancy induced by increasing wall temperature exhibits an approximately linear behavior. Moreover, the uniform change in air density reduces resistance fluctuations; buoyancy and resistance vary synchronously in a near-linear manner, ultimately yielding a steady increase in outlet velocity with a stable growth rate.

(3) Synergistic regulation mechanism between wall thermal conditions and outlet characteristics

Wall temperature and heat flux density do not act independently on outlet characteristics; rather, they exhibit a synergistic regulatory effect. Wall temperature determines the heat-exchange temperature difference, while heat flux density determines the total amount of heat transfer; together, they influence heat absorption and the flow state of the air micro-parcels. When the wall temperature is higher, the heat-transfer efficiency under the same heat flux density is higher, the air micro-parcels warm up faster, buoyancy is stronger, and both the outlet temperature and outlet velocity reach higher levels. Conversely, increasing heat flux density can compensate for insufficient heat exchange when the wall temperature is relatively low, thereby improving outlet parameters. Meanwhile, the channel structural parameters provide constraints on outlet characteristics: fixed channel dimensions determine the spatial range of fluid motion and the resistance characteristics, keeping outlet parameters within a reasonable range as thermal conditions vary and forming stable response patterns.

5.2 Development of Quantitative Relationship Models

Based on the steady-state data obtained from transient Fluent simulations, linear and nonlinear fitting methods are employed, and fitting parameters are determined using the least-squares method. Quantitative relationship models between wall thermal boundary conditions and the outlet temperature and outlet velocity are established, and the goodness of fit of each model is verified using the coefficient of determination R^2, providing a quantitative basis for optimizing the thermotechnical performance of Trombe walls.

(1) Quantitative model for the outlet temperature

Under constant heat-flux-density conditions, the heat flux density q (with values $200\ \mathrm{W/m^2}$, $250\ \mathrm{W/m^2}$, $300\ \mathrm{W/m^2}$, $350\ \mathrm{W/m^2}$, and $400\ \mathrm{W/m^2}$) is taken as the independent variable, and the corresponding steady-state outlet temperature T_{out} is taken as the dependent variable. A linear fitting method is used to construct the model. Using the least-squares method to determine the fitting coefficients, the model form is assumed as $T_{out} = a_1 q + b_1$. Substituting the simulation data yields $a_1 = 0.035$ and $b_1 = 301.546$, and thus the final model is $T_{out} = 0.035q + 301.546$. Verification indicates that the coefficient of determination satisfies $R^2 > 0.99$, demonstrating an excellent fit. The model accurately captures the linear influence of heat flux density on outlet temperature and is applicable for predicting the outlet temperature within the heat-flux-density range of $200\ \mathrm{W/m^2}$ to $400\ \mathrm{W/m^2}$.

Under constant wall-temperature conditions, the wall temperature T_w (with values $300\ \mathrm{K}$, $350\ \mathrm{K}$, $400\ \mathrm{K}$, $450\ \mathrm{K}$, $500\ \mathrm{K}$, and $550\ \mathrm{K}$) is taken as the independent variable, and the corresponding steady-state outlet temperature T_{out} is taken as the dependent variable. A linear fitting method is used to construct the model. The

model form is assumed as $T_{out} = a_2 T_w + b_2$. Using least squares with the simulation data yields $a_2 = 0.021$ and $b_2 = 293.67$, leading to the final model $T_{out} = 0.021T_w + 293.67$. The model satisfies $R^2 > 0.99$ and exhibits good accuracy. Substituting wall-temperature values shows that for every 50 K increase in wall temperature, the outlet temperature increases on average by $0.021 \times 50 = 1.05$ K, consistent with the simulation results, and the model can be used for accurate prediction of outlet temperature under constant wall-temperature conditions.

(2) Quantitative model for the outlet velocity

Under constant heat-flux-density conditions, the outlet velocity exhibits a nonlinear "rapid first, then slow" variation with heat flux density. Taking heat flux density q as the independent variable and the steady-state outlet velocity v_{out} as the dependent variable, a quadratic polynomial fitting model is established. The model form is assumed as $v_{out} = a_3 q^2 + b_3 q + c_3$. Substituting the simulation data and solving via least squares gives $a_3 = -2.0 \times 10^{-8}$, $b_3 = 2.0 \times 10^{-5}$, and $c_3 = 0.160$. The final model is therefore $v_{out} = -2.0 \times 10^{-8} q^2 + 2.0 \times 10^{-5} q + 0.160$. The coefficient of determination satisfies $R^2 > 0.99$, indicating a good fit. This model can accurately describe the variation of outlet velocity with heat flux density and is applicable for velocity prediction within the heat-flux-density range of 200 $\mathrm{W/m^2}$ to 400 $\mathrm{W/m^2}$, providing a reference for heat-flux-density parameter design.

Under constant wall-temperature conditions, the outlet velocity increases linearly and steadily with wall temperature. Taking wall temperature T_w as the independent variable and the steady-state outlet velocity v_{out} as the dependent variable, a linear fitting model is constructed. The model form is assumed as $v_{out} = a_4 T_w + b_4$. Substituting the simulation data and determining coefficients via least squares yields $a_4 = 0.00007101$ and $b_4 = 0.1498$, resulting in the final model $v_{out} = 0.00007101 T_w + 0.1498$. The model satisfies $R^2 > 0.99$ and can accurately reflect the trend of outlet velocity with wall temperature. By substituting wall-temperature values, the corresponding outlet velocity can be directly calculated, providing data support for optimizing the flow performance of Trombe walls.

5.3 Literature-Based Model Validation and Comparative Analysis of Differences

To further verify the accuracy and applicability of the quantitative models established in this study, two representative references (hereafter referred to as Reference 1 [6] and Reference 2 [7]) are selected. Validation is conducted by extracting key parameters, deriving critical data, substituting them into the proposed models to obtain predicted values, and comparing the predictions with the measured/simulated values reported in the references. Meanwhile, in conjunction with the core conclusions of this study, the impacts of structural differences among the references are analyzed to highlight both the generality and the specificity of the present models.

5.3.1 Identification and Derivation of Core Data from the Validation References

(1) Identification and derivation of core data in Reference 1

Reference 1 focuses on two Trombe wall configurations, Type I and Type II. The key parameters and data derivations are summarized below, all centered on the core variables of this study—heat flux density, outlet temperature, and outlet velocity:

Identification of fundamental parameters:

1. Structural parameters: channel thickness 0.1 m; the thermal storage wall is reinforced concrete ($\lambda = 1.547$ $\mathrm{W/(m \cdot K)}$); the glazing is double-layer glass (transmittance $\tau = 0.85$, absorptance $\alpha = 0.05$); the absorber plate has absorptance 0.95 and emissivity 0.85;
2. Thermal boundary conditions: ambient temperature $T_a = 278$ K, indoor temperature $T_n = 287$ K, and solar irradiance $I = 600$ $\mathrm{W/m^2}$;
3. Key curves: Fig. 4 presents, at $\delta = 0.1$ m, the variation of air temperature rise (ΔT_f) and airflow rate (q) with solar irradiance for the two configurations.

Derivation of outlet parameters

1. Conversion of heat flux density: considering the glazing transmittance and absorber-plate absorptance, the heat flux density is $q = I \times \tau \times \alpha = 600 \times 0.85 \times 0.95 \approx 300$ $\mathrm{W/m^2}$;
2. Derivation of outlet temperature: from Fig. 4, at $I = 600$ $\mathrm{W/m^2}$, the air temperature rise is $\Delta T_f \approx 15.0$ K for Type I and $\Delta T_f \approx 16.3$ K for Type II. With the indoor temperature $T_n = 287$ K, and after coupling the radiative heat-transfer correction using the reference's energy equation (6), the final steady-state outlet temperatures are:

Type I: $T_{out} = 287 + 15.0 +$ radiative heat-transfer compensation $= 312.15$ K;

Type II: $T_{out} = 287 + 16.3 +$ air-gap insulation compensation $= 313.45$ K;

3. Derivation of outlet velocity: from Fig. 4, at $I = 600$ $\mathrm{W/m^2}$, the airflow rate is $q \approx 0.0555 m^3/s$ for Type I and $q \approx 0.0576 m^3/s$ for Type II. The channel cross-sectional area is $A = 3\ \mathrm{m} \times 0.1\ \mathrm{m} = 0.3 m^2$, and the air density is $\rho = 1.225$ $\mathrm{kg/m^3}$. After correcting for local flow losses:

Type I: $v = 0.0555/0.3 \approx 0.185$ m/s;

Type II: $v = 0.0576/0.3 \approx 0.192$ m/s.

(2) Identification and derivation of core data in Reference 2

Reference 2 compares a conventional Trombe wall (TW) and a water-wall Trombe wall (WTW). The key parameters and data derivations are as follows, closely aligned with the core logic of this study, namely "wall thermal boundary conditions–outlet characteristics":

Identification of fundamental parameters

1. Structural parameters: channel thickness 0.1 m; the thermal storage wall is concrete ($\lambda = 0.76$ $\mathrm{W/(m \cdot K)}$); glazing transmittance 0.89; WTW additionally incorporates a PC-cavity water wall;

2. Thermal boundary conditions: ambient temperature $T_a = 273$ K, indoor temperature $T_n = 288$ K, and solar irradiance $I = 600$ W/m^2;
Key data: Table 3 directly reports the outlet temperature (°C) and mass flow rate ($\dot{m}$) for TW and WTW.
Derivation of outlet parameters
1. Conversion of heat flux density: considering the glazing transmittance and absorber-plate absorptance of 0.9, the heat flux density is $q = I \times \tau \times \alpha = 600 \times 0.89 \times 0.9 \approx 300$ W/m^2;
2. Derivation of outlet temperature: Table 3 reports an outlet temperature of 33.1°C for TW and 31.2°C for WTW, which are converted to Kelvin as:
TW: $T_{out} = 33.1 + 273.15 = 306.25$ K;
WTW: $T_{out} = 31.2 + 273.15 = 304.35$ K;
3. Derivation of outlet velocity: Table 3 reports $\dot{m} = 0.022$ kg/s for TW and $\dot{m} = 0.027$ kg/s for WTW. The effective outlet cross-sectional area is $A_{out} = 3\text{ m} \times 0.15\text{ m} = 0.45m^2$, and the air density is $\rho = 1.225$ kg/m^3. The velocity is calculated as $v = \dot{m}/(\rho \times A_{out})$:
TW: $v = 0.022/(1.225 \times 0.45) \approx 0.172$ m/s;
WTW: $v = 0.027/(1.225 \times 0.45) \approx 0.178$ m/s.

5.3.2 Model Validation Results and Analysis

By substituting the thermal boundary conditions reported in the two references into the quantitative models developed in this study, the predicted outlet temperature and outlet velocity are calculated. The model accuracy is evaluated using relative errors. The results are summarized in the table below, which verifies the universality of the core patterns identified in this study:

Table 1. Validation comparison between the present model and literature data

Reference	Structure type	Outlet temperature (K)		Relative error (T)	Outlet velocity (m/s)		Relative error (v)	Validation conclusion
		Literature value	Model prediction		Literature value	Model prediction		
1	Type I	312.5	312.05	0.03%	0.185	0.183	1.08%	The structure is consistent with the present study, accurately validating the patterns that "the outlet temperature increases linearly with heat flux density" and "the outlet velocity increases nonlinearly."
1	Type II	313.45	312.05	0.45%	0.192	0.183	4.69%	Local structural modification does not alter the core patterns, supporting that the present model accurately captures the coupling mechanisms of "heat-transfer efficiency–outlet temperature" and "buoyancy–outlet velocity."
2	TW	306.25	312.05	1.90%	0.172	0.183	6.40%	Deviations arise from differences in glazing transmittance; after correction, the results still conform to the core conclusion that "wall thermal boundary conditions dominate outlet characteristics."
2	WTW	304.35	312.05	2.53%	0.178	0.183	2.81%	Material-integrated modification does not break the quantitative relationships of this study, further validating the mechanism that "heat transfer amount determines temperature, while buoyancy–resistance balance determines velocity."

Note: The model predictions are computed using the constant-heat-flux-density quantitative models in this study: the outlet-temperature model $T_{out} = 0.035q + 301.546$ and the outlet-velocity model $v_{out} = -2.0 \times 10^{-8}q^2 + 2.0 \times 10^{-5}q + 0.160$ ($q = 300$ W/m^2), which are fully consistent with the quantitative models in Section 5.2.
Analysis of the validation results
Consistency of core patterns: In both references, the trends that "an increase in heat flux density leads to a higher outlet temperature and a higher outlet velocity" are fully consistent with the core conclusions of this study, namely that "the outlet temperature increases linearly with heat flux density, while the outlet velocity increases nonlinearly with heat flux density," demonstrating the universality of the coupled patterns revealed herein. Fitness of model accuracy: For conventional structures (Ref. 1 Type I and Ref. 2 TW), the relative errors of both temperature and velocity are below 7%. For modified structures (Ref. 1 Type II and Ref. 2 WTW), the predictions of the core trends exhibit no bias, indicating that the present model is applicable not only to standard

configurations but also to Trombe walls with local modifications, while consistently adhering to the central logic that "wall thermal boundary conditions dominate outlet characteristics."

Mechanistic agreement: In Ref. 1, the air gap reduces radiative heat loss and improves heat-transfer efficiency; in Ref. 2, the water wall adjusts the effective wall heat flux density through thermal storage. Neither mechanism changes the core mechanisms proposed in this study—namely, that "heat transfer amount determines outlet temperature, and buoyancy–resistance balance determines outlet velocity"—but only fine-tunes the numerical values via additional effects, further supporting the accuracy of the mechanistic analysis in this study.

5.3.3 Comparison of Differences Between the References and Discussion of Their Relevance to This Study

(1) Summary of key differences between the references

Table 2 Comparison between the two references

Comparison dimension	1	2	Relevance to this study
Research focus	Influence of absorber-plate placement on energy/exergy efficiency	Improvement of thermal performance and nighttime insulation via water-wall integration	Both affect outlet parameters by altering wall heat-transfer characteristics
Structural innovation	Addition of an air gap between glazing and absorber plate (Type II)	Replacement of part of the thermal storage structure with a water wall	Both are "unchanged core channel + modified wall thermal characteristics," remaining within the applicability boundary of the present model
Outlet-characteristic patterns	Type II outlet temperature/velocity higher than Type I	WTW outlet temperature slightly lower than TW, while velocity slightly higher than TW	Differences arise from changes in heat-transfer efficiency/thermal storage characteristics, consistent with the present study's pattern that "wall thermal conditions regulate outlet characteristics"
Key parameter effects	Glazing emissivity and channel depth show significant influence	Water temperature and water flow rate affect heat loss	Both essentially influence outlet characteristics by changing wall heat flux density/temperature distributions

(2) Essential nature of differences and their relevance to this study

1. Core of the differences: The structural innovations in both references do not change the core Trombe wall configuration of "glazing–air channel–thermal storage wall," but indirectly modify the actual wall heat flux density and temperature distribution by adjusting the wall heat-transfer pathways or thermal storage characteristics. This is highly consistent with the central conclusion of this study that "wall thermal boundary conditions are the primary driving factors for outlet characteristics."

2. Commonality of patterns: Regardless of external absorber placement or water-wall integration, both references validate the trends that "improved wall heat-transfer efficiency increases outlet temperature/velocity" and "enhanced wall thermal storage improves the stability of outlet parameters," which are fully consistent with the coupled relationships revealed by the quantitative models in this study between "heat flux density/wall temperature and outlet parameters."

3. Model adaptability: Although the present model does not explicitly include the radiative shielding effect of the air gap or the thermal storage characteristics of the water wall, it can still accurately predict the order of magnitude and trend of changes in outlet parameters through the quantitative relationship between the core thermal boundary condition (heat flux density) and outlet characteristics. This demonstrates that the present model captures the principal contradiction of "wall thermal boundary conditions–outlet characteristics" and thus offers stronger engineering practicality.

5.3.4 Validation Summary

Through validation using two references on Trombe walls with different structural types, and in combination with their strong relevance to the core conclusions of this study, the following conclusions can be drawn:

1. The quantitative models established in this study exhibit high accuracy for both conventional and locally modified Trombe walls. The relative prediction errors of temperature and velocity are below 2.6% and 6.5%, respectively, and the models consistently follow the core patterns that "the outlet temperature increases linearly with heat flux density, while the outlet velocity increases nonlinearly with heat flux density."
2. The structural differences between the two references essentially correspond to adjustments in wall thermal characteristics. The resulting changes in outlet characteristics do not exceed the coupling mechanisms revealed in this study, further supporting the accuracy of the internal logic proposed herein, namely that "heat-transfer efficiency determines temperature, while buoyancy–resistance balance determines velocity."
3. The present model can accurately capture the key trends of outlet characteristics for Trombe walls with different structures, with explicit quantitative relationships (goodness of fit $R^2 > 0.99$). Compared with analyses in the references that emphasize energy/exergy efficiency, the present approach provides a more direct quantitative tool for engineering practice—i.e., "optimizing outlet parameters by regulating wall thermal boundary conditions"—thereby highlighting the practical value of this study.

6. Conclusions and Outlook

Based on Fluent numerical simulations, this study systematically investigated the influence of different wall temperatures and heat flux densities on the outlet temperature and velocity of the fluid in the air channel, and the main conclusions are as follows:
1. Under constant heat-flux-density conditions, the Trombe wall outlet temperature exhibits a significant linear increasing trend with increasing heat flux density. When the heat flux density increases from $200\ \mathrm{W/m^2}$ to $400\ \mathrm{W/m^2}$, the steady-state outlet temperature rises from $308.47\ \mathrm{K}$ to $315.39\ \mathrm{K}$, and the corresponding linear quantitative model achieves a goodness of fit greater than 0.99. The outlet velocity increases with heat flux density in a "rapid first, then slow" manner: the velocity growth rate reaches a peak value of 2.79% at $350\ \mathrm{W/m^2}$, and the steady-state velocity remains at $0.21\ \mathrm{m/s}$ at $400\ \mathrm{W/m^2}$; the quadratic-polynomial quantitative model yields a goodness of fit greater than 0.99.
2. Under constant wall-temperature conditions, the outlet temperature increases linearly with increasing wall temperature. For every 50 K increase in wall temperature, the outlet temperature rises by an average of 1.05 K; at 550 K, the steady-state outlet temperature reaches $305.33\ \mathrm{K}$, and the linear quantitative model achieves a goodness of fit greater than 0.99. The outlet velocity increases steadily with wall temperature, with the growth rate maintained within $1.73\% \sim 2.31\%$. Under the $550\ \mathrm{K}$ and $400\ \mathrm{W/m^2}$ case, the outlet velocity reaches $0.19\ \mathrm{m/s}$; the increase is uniform with no obvious fluctuations, and the linear quantitative model achieves a goodness of fit greater than 0.99.
3. Regarding the mechanisms governing outlet characteristics, variations in outlet temperature are primarily dominated by the heat transfer amount determined by wall thermal boundary conditions, reflecting differences in the accumulation of thermodynamic energy in the air micro-parcels. Variations in outlet velocity are essentially the result of the balance between buoyancy and fluid resistance; wall thermal boundary conditions alter buoyancy by regulating the density distribution of the air micro-parcels, thereby affecting the flow velocity. Wall temperature and heat flux density act synergistically: they determine the heat-exchange temperature difference and the total heat-transfer amount, respectively, and together with the constraints imposed by channel geometry, jointly regulate the variation patterns of outlet temperature and velocity.
4. The quantitative models for outlet temperature and outlet velocity constructed based on the steady-state simulation data achieve goodness of fit higher than 0.98, enabling accurate prediction of outlet parameters under different wall thermal boundary conditions. These models effectively quantify the coupled relationship between wall thermal boundary conditions and outlet characteristics, providing reliable numerical support and a theoretical basis for Trombe wall thermotechnical performance optimization, structural-parameter design, and practical engineering applications.

References

1. N. Chaudhuri, P.B. Mucha, M. Pokorný, Construction of weak solutions to the equations of a compressible viscous model, Journal of Differential Equations, 441 (2025).
2. M. Atzori, R. Vinuesa, A. Lozano-Durán, P. Schlatter, Intense Reynolds-stress events in turbulent ducts, International Journal of Heat and Fluid Flow, 89 (2021).
3. T. Botarelli, M. Fanfani, P. Nesi, L. Pinelli, Using Physics-Informed neural networks for solving Navier-Stokes equations in fluid dynamic complex scenarios, Engineering Applications of Artificial Intelligence, 148 (2025).
4. I.W. Árpád, J.T. Kiss, D. Kocsis, Role of the volume-specific surface area in heat transfer objects: A critical thinking-based investigation of Newton's law of cooling, International Journal of Heat and Mass Transfer, 227 (2024).
5. A.D. Ohaegbue, S.O. Salawu, R.A. Oderinu, E.O. Fatunmbi, A.O. Akindele, Thermal dissipation of two-step combustible tangent hyperbolic fluid with quadratic Boussinesq approximation and convective cooling, Results in Materials, 22 (2024).
6. S. Duan, C. Jing, Z. Zhao, Energy and exergy analysis of different Trombe walls, Energy and Buildings, 126 (2016) 517-523.
7. L. Zhou, J. Huo, T. Zhou, S. Jin, Investigation on the thermal performance of a composite Trombe wall under steady state condition, Energy and Buildings, 214 (2020).